

# Stratospheric water vapor and ozone response to different QBO disruption events in 2016 and 2020

Mohamadou Diallo<sup>1</sup>, Felix Ploeger<sup>1,2</sup>, Michaela I. Hegglin<sup>3</sup>, Manfred Ern<sup>1</sup>,  
Jens-Uwe Grooß<sup>1</sup>, Sergey Khaykin<sup>4</sup> and Martin Riese<sup>1,2</sup>

<sup>1</sup>Institute of Energy and Climate Research, Stratosphere (IEK-7), Forschungszentrum Jülich, 52 425 Jülich, Germany.

<sup>2</sup>Institute for Atmospheric and Environmental Research, University of Wuppertal, Wuppertal, Germany.

<sup>3</sup>Department of Meteorology, University of Reading, Reading, UK.

<sup>4</sup>Laboratoire Atmosphères, Milieux, Observations Spatiales, UMR CNRS 8190, IPSL, Sorbonne Univ./UVSQ, Guyancourt, France.

## Key Points:

- The QBO disruptions in both 2016 and 2020 decreased lower stratospheric water vapor and ozone.
- There are significant differences in the strength and depth of the impacts of the two QBO disruption events due to differences in tropical upwelling and cold point temperature.
- The differences in tropical upwelling and cold point temperature are caused by stronger planetary and gravity wave breaking in the lower stratosphere in 2016 than in 2020.

---

Corresponding author: Mohamadou Diallo, [m.diallo@fz-juelich.de](mailto:m.diallo@fz-juelich.de)

## Abstract

The Quasi-Biennial Oscillation (QBO) is a major mode of climate variability with periodically descending westerly and easterly winds in the tropical stratosphere, modulating transport and distributions of key greenhouse gases such as water vapor and ozone. In 2016 and 2020, anomalous QBO easterlies disrupted the QBO's 28-month period previously observed. Here, we quantify the impact of these QBO disruptions on lower stratospheric circulation, and water vapour and ozone using reanalyses and satellite observations, respectively. Both constituents decrease globally from early spring to late autumn during 2016, while they only weakly decrease during 2020. These dissimilarities result from differences in upwelling and cold-point tropopause temperatures caused by anomalous planetary and gravity wave forcing. Our results highlight the need for a better understanding of the causes of QBO disruptions, their interplay with other modes of climate variability, and their impacts on water vapor and ozone in the face of a changing climate.

## Plain Language Summary

The Quasi-Biennial Oscillation (QBO) is one of the key atmospheric modes of climate variability as it modulates the stratospheric Brewer-Dobson circulation (BDC) and composition in the stratosphere and troposphere. The quasi-periodic pattern of alternating QBO easterlies and westerlies was subject to two disruptions during the 2015–2016 and 2019–2020 winters, therefore, leading to lower stratospheric anomalous circulation and composition. Besides similarities in many respects, our analysis shows differences in the strength and depth of the stratospheric circulation and upper troposphere/lower stratosphere (UTLS) composition response to the 2015–2016 and 2019–2020 QBO disruptions. These differences are mainly caused by differences in the the strength and depth of the forcing of the atmospheric circulation by planetary and gravity waves, which may be associated with the anomalous regional surface conditions such as the strong El Niño Southern Oscillation (ENSO) in 2015–2016, the strong Indian Ocean Dipole (IOD) as well as the particularly warmer stratosphere of the Southern Hemisphere midlatitudes linked to Australian wildfire smoke in 2019–2020. Our results suggest a need of better understanding the interplay between QBO phases, ENSO events and IOD events in future climate change as it may have a large impact on the UTLS composition and its changes.

## 1 Introduction

The upper troposphere and lower stratosphere (UTLS) is a key region of the Earth climate system because of its large sensitivity to radiative forcing of greenhouse gases, such as water vapor ( $\text{H}_2\text{O}$ ) and ozone ( $\text{O}_3$ ) (Gettelman et al., 2011; Dessler et al., 2013; Nowack et al., 2015). Any changes in the composition of these radiatively active trace gases in the UTLS region lead to large impact on surface climate (e.g., Forster & Shine, 2002, 1999; Solomon et al., 2010; Riese et al., 2012). Ozone is mainly produced in the middle stratosphere and is a good proxy of the tropical upwelling. In addition, ozone variability in the tropical lower stratosphere is affected by variability in tropical upwelling (Randel et al., 2007; Abalos et al., 2013). The ozone transport and lifetime in the UTLS region are both modulated by the seasonality in the stratospheric circulation and the natural modes of climate variability, including the Quasi-Biennial Oscillation (QBO) (Randel & Thompson, 2011; Diallo et al., 2018). Lower stratospheric water vapor and its multi-timescale variations ranging from day to decades are mainly controlled by changes in the tropical cold point tropopause temperatures and its modulations by the natural variability, including the QBO (Holton & Gettelman, 2001; Hu et al., 2016; Tao et al., 2019). Therefore, the amount of water vapor in the UTLS region is directly linked to the dehydration in the air parcels crossing through the coldest temperatures in the tropical tropopause layer (e.g., between 14 and 19 km; Fueglistaler et al., 2009).

69 Considered as a dominant mode of variability of the equatorial stratosphere, the  
70 QBO globally impacts the transport and distributions of stratospheric water vapor and  
71 ozone. Mostly driven by gravity waves and equatorially trapped waves, the QBO is a quasi-  
72 periodic oscillation between tropical westerly and easterly zonal wind shears (Baldwin  
73 et al., 2001; Ern et al., 2014). Both phases modulate the vertical and meridional com-  
74 ponents of the stratospheric circulation and affect temperature structure, therefore, im-  
75 pacting the water vapor and ozone composition and radiative feedback in the UTLS re-  
76 gion (Niwano et al., 2003; Diallo et al., 2019).

77 The quasi-periodic QBO cycle of about 28-month period, which alternates between  
78 westerly and easterly zonal wind shears, was subject to two disruptions in the past five  
79 years. In January 2016 and 2020, the anomalous QBO westerlies in the tropical lower  
80 stratosphere were unexpectedly interrupted by anomalous QBO easterlies created by com-  
81 bination of planetary waves propagating from the middle latitudes and equatorial con-  
82 vective gravity waves (Osprey et al., 2016; Coy et al., 2017; Hitchcock et al., 2018; Kang  
83 et al., 2020; Kang & Chun, 2021). There is not yet a clear understanding of how these  
84 QBO disruptions are linked to anomalously warm or cold sea surface temperatures (Taguchi,  
85 2010; Schirber, 2015; Dunkerton, 2016; Christiansen et al., 2016; Barton & McCormack,  
86 2017), volcanic aerosols (Kroll et al., 2020; DallaSanta et al., 2021), wildfire smoke (Khaykin  
87 et al., 2020; Yu et al., 2021) and climate changes (Anstey et al., 2021a). However, re-  
88 cent study based on climate model simulations from phase six of the Coupled Model In-  
89 tercomparison Project (CMIP6) predicts increased disruption frequencies to the quasi-  
90 regular QBO cycle in a changing climate (Osprey et al., 2016; Anstey et al., 2021a). Pre-  
91 vious studies also suggest that the QBO amplitude in the tropical stratosphere is decreas-  
92 ing in the lower stratosphere due to the climate change-induced strengthening of tropi-  
93 cal upwelling (Saravanan, 1990; Kawatani et al., 2011; Kawatani & Hamilton, 2013). Thus,  
94 in the context of a changing climate, the predictable QBO signal associated with the quasi-  
95 regular phase progression and amplitude as well as its potential impacts on UTLS com-  
96 position faces an uncertain future. Therefore, it is of particular importance to quantify  
97 and better understand the different impact of the QBO disruptions on changes in UTLS  
98 water vapor and ozone, which have the potential to impact the global radiative forcing  
99 of climate (Forster & Shine, 1999; Butchart & Scaife, 2001; Solomon et al., 2010; Riese  
100 et al., 2012).

101 Here, we quantify the similarity and differences in the strength and depth between  
102 the 2015–2016 and 2019–2020 QBO disruption impacts on lower stratospheric water vapor  
103 and ozone from satellite observations. Also, we analyse the main drivers of the dif-  
104 ferences in anomalous circulation and UTLS composition changes. Section 2 describes  
105 the satellite observational data sets and the regression model used for the quantification.  
106 Section 3 describes the anomalous stratospheric circulation and UTLS composition changes  
107 following the 2016 and 2020 events. Section 4 discusses the results of a regression anal-  
108 ysis to provide evidence for the impact of the QBO disruptions on stratospheric water  
109 vapor and ozone together with the main reasons of the anomalous circulation and com-  
110 position differences between the 2015–2016 and 2019–2020 QBO disruption impacts re-  
111 lated to planetary and gravity wave dissipation. Finally, we discuss our results in the con-  
112 text of the anomalous surface conditions, including the strong El Niño Southern Oscil-  
113 lation (ENSO) in 2015–2016, the strong Indian Ocean Dipole (IOD) as well as the par-  
114 ticularly warmer stratosphere linked to Australian wildfire smoke in 2020.

## 115 2 Data and methodology

116 To quantify the QBO impact, we used the monthly mean ozone and water vapor  
117 mixing ratios from the Aura Microwave Limb Sounder (MLS) satellite observations cover-  
118 ing the 2013–2020 period (Livesey et al., 2017). The version 4.4 MLS data set used here  
119 has a vertical resolution of 2.5–3 km ranging from 8 to 35 km and 60°S/N with a high  
120 precision and lower systematic uncertainty (Santee et al., 2017). Previous findings show

121 that MLS zonal monthly mean H<sub>2</sub>O mixing ratios show very good agreement with the  
122 multi-instrument mean (Hegglin et al., 2013, 2021).

123 In addition to the MLS data set, we also utilize the temperature ( $T$ ) and zonal mean  
124 wind ( $U$ ) from the ERA5 reanalysis of the European Centre for Medium-Range Weather  
125 Forecasts (ECMWF) (Hersbach et al., 2020). We have also calculated the residual vertical  
126 velocity ( $\overline{w^*}$ ) using the Transformed Eulerian Mean (TEM; Andrews et al. (1987))  
127 and decomposed the wave drag into planetary and gravity wave contributions to the cir-  
128 culation anomalies (Ern et al., 2014, 2021). For more details about the ERA5 TEM cal-  
129 culations and wave decomposition see Diallo et al. (2021).

130 We disentangle the QBO impact on these monthly mean stratospheric water va-  
131 por and ozone mixing ratios from the other sources of natural variability by using a hy-  
132 brid multiple regression model (Eq. 1). This established regression method is appropri-  
133 ate to separate the relative influences of the considered modes of climate variability, in-  
134 cluding the QBO, on stratospheric water vapor and ozone. Additional details about the  
135 prediction model and its applications can be found in Diallo et al. (2018). Our regres-  
136 sion model decomposes the given monthly zonal mean variable,  $Var_i$ , into a long-term  
137 linear trend, seasonal cycle, modes of climate variability and a residual ( $\epsilon$ ). For a given  
138 variable  $Var_i$  (herein O<sub>3</sub>, H<sub>2</sub>O, ( $T$ ),  $\overline{w^*}$ , PWD and GWD), the prediction model yields

$$Var_i(t_{month}, y_{lat}, z_{alt}) = Trend(t_{month}, y_{lat}, z_{alt}) + SeasCyc(t_{month}, y_{lat}, z_{alt}) + \sum_{n=1}^5 b_n(y_{lat}, z_{alt}) \cdot Proxy_n(t_{month} - \tau_n(y_{lat}, z_{alt})) + \epsilon(t_{month}, y_{lat}, z_{alt}), \quad (1)$$

139 where  $Proxy_n$  represents the different climate indexes used here.  $Proxy_1$  is a normal-  
140 ized QBO index (QBOi) from CDAS/Reanalysis zonally averaged winds at 50 hPa (Kalnay  
141 et al., 1996).  $Proxy_2$  is the normalized Multivariate ENSO Index (MEI; Wolter & Tim-  
142 lin, 2011),  $Proxy_3$  is the Indian Ocean Dipole (IOD, Saji et al., 1999),  $Proxy_4$  is the Madden-  
143 Julian Oscillation (MJO, Son et al., 2017), and  $Proxy_5$  is the AOD from satellite data  
144 (Thomason et al., 2018).  $Trend(t_{month}, y_{lat}, z_{alt})$  are a linear trend.  $SeasCyc(t_{month}, y_{lat}, z_{alt})$   
145 is the annual cycle. The coefficients are the amplitude  $b_n$  and the lag  $\tau_n(y_{lat}, z_{alt})$  as-  
146 sociated with the QBO, ENSO, IOD, MJO and AOD respectively. The solar forcing is  
147 neglected because our data set is relatively short and covers less than one 11-year solar  
148 cycle. Finally, we estimate the uncertainty in the statistical prediction using a Student's  
149  $t$  test technique (von Storch & Zwiers, 1999; Friston et al., 2007).

### 150 3 Characterisation of the 2016 and 2020 anomalous circulations

151 In January 2016 and 2020 unexpected tropical QBO easterlies (negative QBOi) de-  
152 veloped in the center of the tropical QBO westerlies, thereby breaking the quasi-regular  
153 QBO cycle of alternating easterly and westerly phases (Osprey et al., 2016; Newman et  
154 al., 2016; Anstey et al., 2021b). Both QBO disruptions have been associated with a com-  
155 bination of extratropical Rossby waves, equatorial planetary waves (Kelvin, Rossby, mixed  
156 Rossby-gravity, and inertia-gravity), and small-scale convective gravity waves, propa-  
157 gating into the deep tropics and depositing their negative momentum forcing (Osprey  
158 et al., 2016; Newman et al., 2016; Kang et al., 2020; Kang & Chun, 2021). Although sim-  
159 ilar in many respects, including the causes of the sudden development of tropical QBO  
160 easterlies in the center of tropical QBO westerlies, the two disruptions also exhibit dif-  
161 ferences, in particular how the wave forcing triggered the events as in the structure (strength  
162 and depth) of the impacts and the level at which it started. While the 2015–2016 QBO  
163 disruption is primarily triggered by mid-latitude Rossby waves propagating from the north-  
164 ern hemisphere into the deep tropics, the 2019–2020 QBO disruption is initially triggered  
165 by the equatorial planetary and small-scale convective gravity waves propagating into  
166 the UTLS (Kang et al., 2020; Kang & Chun, 2021).

167 The similarities as well as the differences between the two disruption events are also  
 168 visible in the inter-annual variability of the tropical lower stratospheric zonal mean wind  
 169 (a), H<sub>2</sub>O (b) and O<sub>3</sub> (c) anomalies as a percentage change relative to the monthly mean  
 170 mixing ratio during the 2013–2020 period (Fig. 1a–c). Both QBO disruptions are expected  
 171 to impact the tropical upwelling, via wave–mean–flow interaction (Holton, 1979; Dunker-  
 172 ton, 1980; Grimshaw, 1984) and control of the tropical cold point temperatures (Kim  
 173 & Son, 2012; Kim & Alexander, 2015). This impact of the 2015–2016 and 2019–2020 QBO  
 174 disruptions on the transport and distribution of lower stratospheric H<sub>2</sub>O (b) and O<sub>3</sub> (c)  
 175 is the most effective when the signal reaches the tropopause level e.g. from June to Au-  
 176 gust (Fig. 1a, d) (Tweedy et al., 2017; Diallo et al., 2018). The zonal mean wind shows  
 177 that the QBO disruption is stronger and deeper in 2015–2016 than in 2019–2020 regard-  
 178 ing the westerly jet at 30 *hPa* (Fig. 1a and Fig. S1a–b in the supplement). The 2019–  
 179 2020 QBO disruption shows a clear cut of the westerlies in two parts while the 2015–2016  
 180 QBO disruption shifts the westerlies upward (Fig. 1a). As soon as the downward prop-  
 181 agation of tropical QBO easterlies reaches the tropical tropopause ( $\sim 16$  *km*) around June–  
 182 August 2016, the H<sub>2</sub>O mixing ratios start to decrease i.e. turning from positive to neg-  
 183 ative anomalies. As reported by (Diallo et al., 2018), the alignment of the strong El Niño  
 184 event with westerly QBO in early boreal winter of 2015–2016 substantially increased H<sub>2</sub>O  
 185 and decreased O<sub>3</sub> in the tropical lower stratosphere (Fig. 1b, c). Then, the sudden oc-  
 186 currence of the QBO disruption led to a lower stratospheric H<sub>2</sub>O and O<sub>3</sub> decrease from  
 187 late spring to early following winter.

188 Conversely, during the 2019–2020 QBO disruption, Figure 1b, c show clear differ-  
 189 ences in the tropical lower stratospheric trace gas anomalies, particularly in the strength  
 190 and depth of H<sub>2</sub>O and O<sub>3</sub> anomalies consistent with the zonal wind changes (Fig. 1a).  
 191 The tropical lower stratospheric O<sub>3</sub> anomalies are purely responding to the enhanced trop-  
 192 ical upwelling caused by a combination of a strong El Niño event, negative IOD event  
 193 and the QBO disruption in 2015–2016, and caused by a combination of a weak La Niña,  
 194 strong positive IOD event and the QBO disruption in 2019–2020 (e.g., easterly winds  
 195 at 100–40 *hPa*). However, the tropical lower stratospheric H<sub>2</sub>O variability (tape recorder)  
 196 is more challenging to interpret because of its regulation by the variability in the trop-  
 197 ical cold point temperatures (Holton & Gettelman, 2001; Hu et al., 2016). In 2020, the  
 198 QBO disruption–induced tropical lower stratospheric H<sub>2</sub>O anomalies are weaker than  
 199 in 2016, consistent with the zonal mean wind anomalies (Fig. 1a, Fig. S1a–d and Fig. S2a–  
 200 d in the supplement). Particularly, the 2020 tape recorder shows large positive H<sub>2</sub>O anoma-  
 201 lies even after the disruption that are of opposite sign to the 2016 H<sub>2</sub>O anomalies (Fig. 1b,  
 202 c). This complexity in H<sub>2</sub>O inter-annual variability lies in its dependency on the inter-  
 203 play of different modes of natural variability, including the QBO phases (Diallo et al.,  
 204 2018; Tian et al., 2019; Liess & Geller, 2012), seasons (early or late in the winter) and  
 205 location (western, central or eastern Pacific, where the ENSO and IOD maximum oc-  
 206 curs (Garfinkel et al., 2013; Smith et al., 2021)). Therefore, to elucidate the effect of both  
 207 QBO disruptions on the lower stratospheric H<sub>2</sub>O and O<sub>3</sub> anomalies, we performed re-  
 208 gression analysis both without and with explicitly including QBO signals to isolate the  
 209 QBO impact on these trace gases. The difference between the residual ( $\epsilon$  in Eq. 1) with  
 210 and without explicit inclusion of the QBO signals gives the QBO–induced impact on strato-  
 211 spheric H<sub>2</sub>O and O<sub>3</sub> anomalies. This approach of differencing the residuals is similar to  
 212 direct calculations, projecting the regression fits onto the QBO basis functions, i.e., the  
 213 QBO predictor timeseries (see supplement Figs. 2 and 4 in (Diallo et al., 2017)). In ad-  
 214 dition, this differencing approach avoids the need to reconstruct the time series after the  
 215 regression analysis.

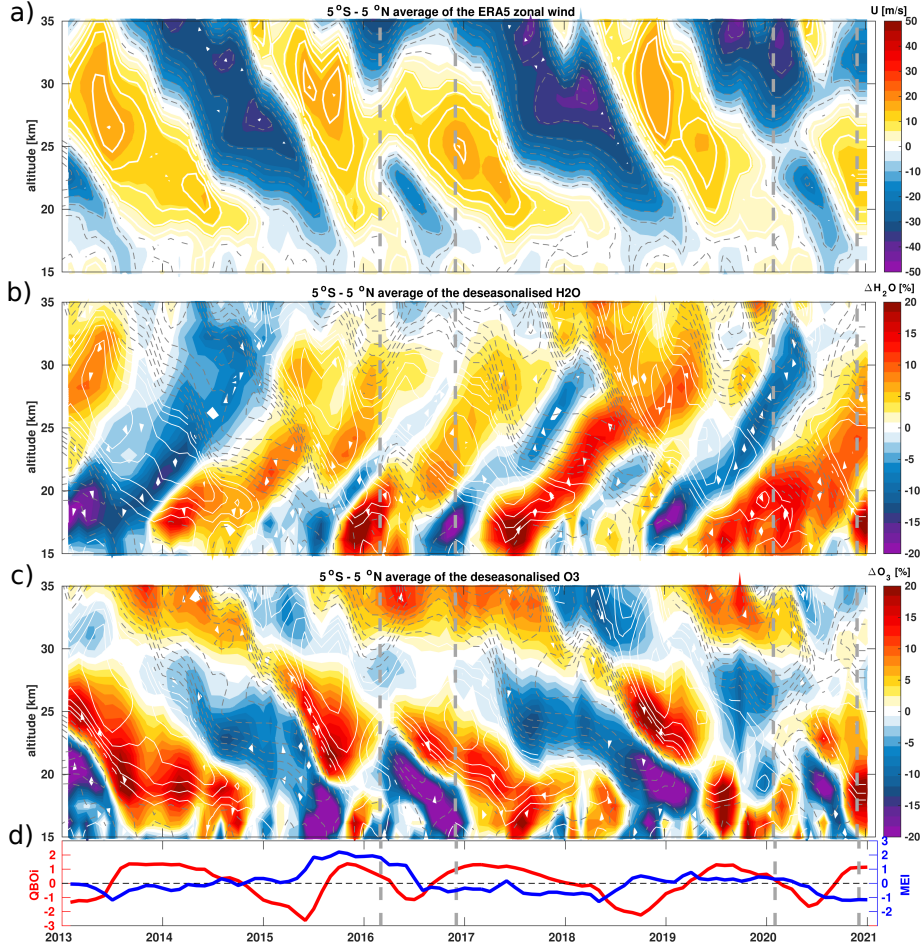


**Figure 1.** Tropical zonal mean zonal wind ( $U$ ) from ERA5 (a) and deseasonalized tropical stratospheric  $H_2O$  and  $O_3$  time series from MLS satellite observations for the 2013–2020 period in percent change from long-term monthly means as a function of time and altitude. (a) Zonal mean wind  $U$ . (b) Deseasonalized monthly mean  $H_2O$  anomalies. (c) Deseasonalized monthly mean  $O_3$  anomalies. Vertical grey dashed lines indicate the QBO disruption onset and offset years. The lowermost panel (d) shows the QBO index at  $50\text{ hPa}$  in red and the MEI index in blue. Monthly averaged zonal mean zonal wind component,  $u$  ( $\text{m s}^{-1}$ ), from ERA5, is overlaid as solid white (westerly) and dashed gray (easterly) lines.

216

## 4 Attribution to drivers using a statistical prediction model

217

### 4.1 Impact of QBO disruptions on UTLS composition

218

219

220

221

222

223

224

225

226

Figures 2a, b show time series of the QBO-induced inter-annual variability in tropical lower stratospheric  $H_2O$  and  $O_3$  anomalies estimated from the difference between the residual ( $\epsilon$  in Eq. 1) without and with explicit inclusion of the QBO proxy for the 2013–2020 period. A footprint of both QBO disruptions is clearly visible in lower stratospheric  $H_2O$  and  $O_3$  anomalies with a shift from positive anomalies related to the westerly winds (positive QBOi) to negative anomalies related to the easterly winds (negative QBOi). The QBO disruption-induced  $O_3$  anomalies are sudden and clearly follow the monthly mean zonal mean wind changes. The QBO disruption-induced  $H_2O$  anomalies are roughly in phase with the zonal wind anomalies with a delay of about 3–6 months

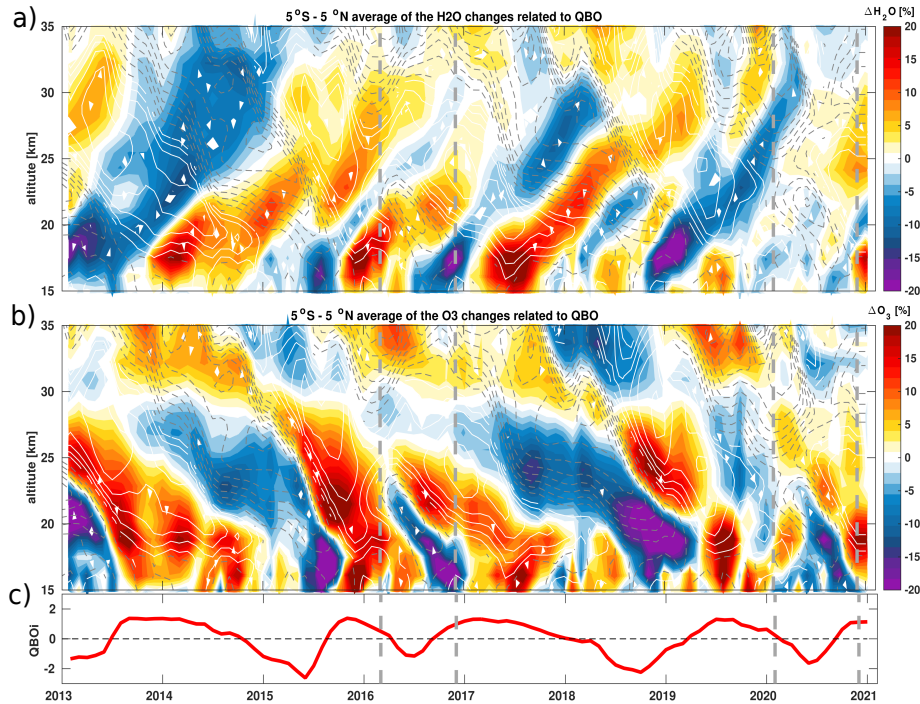


**Figure 2.** QBO impact on the stratospheric H<sub>2</sub>O (a) and O<sub>3</sub> (b) anomalies from the MLS satellite observations for the 2013–2020 period in percent change relative to monthly mean mixing ratios as a function of time and altitude. Shown QBO impact on the stratospheric trace gases is derived from the multiple regression fit as the difference between the residual ( $\epsilon$  in Eq. 1) without and with explicit inclusion of the QBO signal. The lower panel below indicates the QBO index at 50 hPa in red. Vertical grey dashed lines indicate the QBO disruption onset and offset years.

227 because of its tropospheric origin and its tropical cold point temperature anomaly de-  
 228 pendency.

229 Beside the good agreement in the patterns of trace gas changes, there are clear dif-  
 230 ferences in the strength and depth of the lower stratospheric H<sub>2</sub>O and O<sub>3</sub> response to  
 231 the QBO disruptions between the 2016 and the 2020 events. These differences in the im-  
 232 pact of the QBO disruption are consistent with the observed lower stratospheric H<sub>2</sub>O  
 233 and O<sub>3</sub> anomalies (Fig. 1 and Fig. S2a–c). During 2016, the QBO shift from westerlies  
 234 to easterlies at 40 hPa in the tropical lower stratosphere induces substantial negative H<sub>2</sub>O  
 235 and O<sub>3</sub> anomalies as large as 15%–20% between 16 and 20 km from the early boreal spring  
 236 to the next boreal winter. This decrease in H<sub>2</sub>O and O<sub>3</sub> mixing ratios is consistent with  
 237 upward transport of young and dehydrated air poor in H<sub>2</sub>O and O<sub>3</sub> into the lower strato-  
 238 sphere (Fig. 2). As expected, the sudden occurrence of the QBO disruption causes anom-  
 239 alously cold point temperatures and stronger tropical upwelling, consistent with the strong  
 240 decrease in H<sub>2</sub>O and O<sub>3</sub> mixing ratios.

241 However, besides the similarities in the structural changes, the QBO disruption induced-  
 242 negative H<sub>2</sub>O and O<sub>3</sub> anomalies are smaller and shallower in 2020 than in 2016. The dif-  
 243 ferences in the magnitude of negative O<sub>3</sub> anomalies suggest a weaker tropical upwelling  
 244 anomalies of the stratospheric circulation in 2020 than in 2016, consistent with the dif-  
 245 ferences in the strength and depth of the wave forcing anomalies discussed in Sect. 4.2.

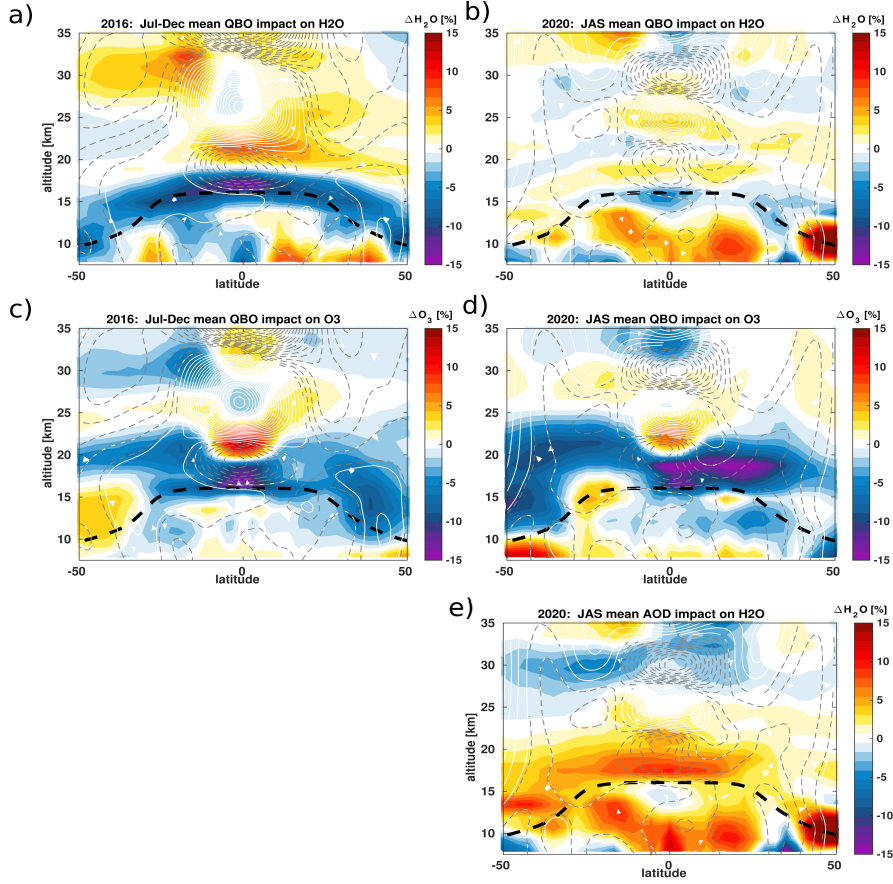


**Figure 3.** Zonal mean impact of the QBO disruption on the lower stratospheric H<sub>2</sub>O (a, b) and O<sub>3</sub> (c, d) anomalies from MLS satellite observations averaged from July to December for 2016 (a, c) and from July to September for 2020 (b, d) period. In addition, the impact of the 2020 Australian wildfires is shown (e). All panels show the percentage change relative to monthly mean mixing ratios as a function of latitude and altitude. The impact of the QBO disruptions and the Australian wildfire on the stratospheric trace gases is derived from the multiple regression fit as the difference between the residual ( $\epsilon$  in Eq. 1) without and with explicit inclusion of the QBO signal. The black dashed horizontal line indicates the tropopause from ERA5. Monthly mean zonal mean wind component,  $u$  ( $\text{m s}^{-1}$ ), from ERA5 is overlaid as solid white (westerly) and dashed gray (easterly) lines.

246 The differences in the strength of H<sub>2</sub>O anomalies suggest that the impact of QBO dis-  
 247 ruptions on tropical cold point temperatures is substantially different between the year  
 248 2016 and year 2020. In addition, we note that the early QBO westerly followed by the  
 249 shift to QBO easterly is not the main cause of the large increase in the 2020 lower strato-  
 250 spheric H<sub>2</sub>O anomalies. In the following, we assess the potential impact of the unusu-  
 251 ally strong Australian wildfire smoke on the lower stratospheric H<sub>2</sub>O anomalies in 2020  
 252 (Khaykin et al., 2020; Yu et al., 2021).

253 Figures 3a–b show the zonal mean impact of the QBO disruptions on lower strato-  
 254 spheric H<sub>2</sub>O and O<sub>3</sub> anomalies. Figure 3e shows the impact of 2020 Australian wildfire  
 255 AOD on lower stratospheric H<sub>2</sub>O and O<sub>3</sub> anomalies. The lower stratospheric H<sub>2</sub>O anoma-  
 256 lies are averaged from July to December for 2016 and from July to September for 2020

257 respectively. We chose different averaging periods for 2016 and 2020 because of the dif-  
 258 ferences in the strength and depth of the QBO disruption-induced H<sub>2</sub>O and O<sub>3</sub> anoma-  
 259 lies. These chosen periods highlight better the similarities in patterns and maximum occur-  
 260 rence of the QBO impact on both trace gas anomalies as well as the differences in the  
 261 strength and depths of H<sub>2</sub>O and O<sub>3</sub> responses.

262 In 2016, the shift to QBO easterly phase in the tropics significantly dehydrates the  
 263 global lower stratosphere by about 10 to 15 % below 20 km (Fig. 3a and Fig. S2a) (Di-  
 264 allo et al., 2018; Tweedy et al., 2017). This decrease in H<sub>2</sub>O mixing ratios is due to the  
 265 enhanced tropical upwelling and related decrease of cold point temperature as discussed  
 266 later in Sect. 4.2 (Jensen et al., 1996; Hartmann et al., 2001; Geller et al., 2002; Schoe-  
 267 berl & Dessler, 2011). Because of the asymmetry of the mean meridional mass circula-  
 268 tion, which is driven by planetary wave activity (e.g. Holton & Gettelman, 2001) and  
 269 eddy mixing (e.g. Haynes & Shuckburgh, 2000), the rising dehydrated air from the trop-  
 270 ics moves toward middle and high latitudes of both hemispheres. The positive H<sub>2</sub>O anoma-  
 271 lies above 20 km are related to the effect of the preceding QBO westerly phase on TTL  
 272 temperatures and the upward propagating tape-recorder signal. The changes in H<sub>2</sub>O anoma-  
 273 lies are consistent with the observed tropical negative O<sub>3</sub> anomalies below 20 km induced  
 274 by the QBO easterly phase and indicate an enhanced tropical upwelling in the lower strato-  
 275 sphere (Fig. 3c and Fig. S2c in the supplement). Above 20 km, the positive tropical O<sub>3</sub>  
 276 anomalies are associated with the QBO westerly phase between ((Fig. 3c and Fig. S2c  
 277 in the supplement). Also note the large variability in extratropical O<sub>3</sub> anomalies related  
 278 to the QBO influence on the extratropical circulation (Damadeo et al., 2014), stratospheric  
 279 major warmings, and chemical processes (WMO, 2018).

280 In 2020, the patterns of QBO disruption-induced changes in tropical lower strato-  
 281 spheric H<sub>2</sub>O and O<sub>3</sub> anomalies exhibit similarities with the 2015–2016 QBO disruption  
 282 effect. Both trace gases show negative anomalies in the tropics, corroborating the en-  
 283 hanced upwelling induced by the shift to QBO easterly phase in the tropics (Fig. 3b and  
 284 Fig. S2b in the supplement). However, there are also large differences in the lower strato-  
 285 spheric trace gas response to the shift from the tropical QBO westerly phase to the trop-  
 286 ical QBO easterly phase, particularly in H<sub>2</sub>O anomalies. Conversely to the globally de-  
 287 hydrated lower stratosphere in 2016, the sudden development of tropical QBO easterly  
 288 in 2020 led to a smaller decrease in lower stratospheric H<sub>2</sub>O mixing ratios, therefore, to  
 289 smaller lower stratospheric H<sub>2</sub>O anomalies (Fig. 3b and Fig. S2b in the supplement). In  
 290 addition to the good agreement in the zonal mean structure of O<sub>3</sub> anomalies between  
 291 both QBO disruptions, the changes in zonal mean O<sub>3</sub> mixing ratios induced by the 2019–  
 292 2020 QBO disruption are also weaker in the tropics than for the 2015–2016 QBO dis-  
 293 ruption. The differences between the 2016 and 2020 H<sub>2</sub>O and O<sub>3</sub> anomalies clearly sug-  
 294 gest substantial differences in the anomalous circulation and the tropical cold point tem-  
 295 peratures. The weak negative tropical O<sub>3</sub> anomalies suggest that the tropical upwelling  
 296 of the stratospheric circulation is slower and weaker in 2020 than in 2016. Simultane-  
 297 ously, the positive tropical H<sub>2</sub>O anomalies in 2020 indicate a warmer tropical cold point  
 298 temperature. The main dynamical causes of these differences are investigated in the fol-  
 299 lowing section.

## 300 4.2 Mechanisms behind the strength and depth differences

301 To further investigate and understand the key drivers of the anomalous circulation  
 302 differences between the 2015–2016 and 2019–2020 QBO disruptions, we analyse the dif-  
 303 ferences in the residual vertical velocity ( $\overline{w^*}$ ) and temperature anomalies. Figure 4a–c  
 304 show tropical time series of the residual circulation vertical velocity and temperature anoma-  
 305 lies together with the QBO disruption impacts on temperature anomalies during the 2015–  
 306 2016 and 2019–2020 periods, respectively. Latitude-altitude sections of the residual cir-  
 307 culation vertical velocity and temperatures together with the QBO disruption impacts  
 308 on temperature anomalies during the 2015–2016 and 2019–2020 periods are shown in the

309 supplement Fig. S3. Clearly, there are substantial differences in the tropical upwelling  
 310 of the stratospheric circulation and temperatures for the two disruption events. In 2016,  
 311 the tropical upwelling strongly increases up to about 20 km when the QBO easterly phase  
 312 reaches the tropopause (Fig. 4a). This enhancement of tropical upwelling during July-  
 313 August-September (JAS) 2016 is also visible in the JAS zonal mean cross section of the  
 314 mean residual vertical velocity and temperature anomalies (Fig S3a, b), together with  
 315 the QBO disruption impacts on temperature anomalies (Fig. S3c in the supplement). How-  
 316 ever, the increase of the tropical upwelling is weaker and shallower in 2020 than in 2016  
 317 (Fig. 4a and Fig. S3a in the supplement). The differences in the anomalous tropical up-  
 318 welling are also consistent with the differences in the QBO disruption-induced temper-  
 319 ature anomalies (Fig. 4a, b and Fig. S3c-f in the supplement). In 2016, the tropical cold  
 320 point temperature anomalies (at altitudes of about 17–18 km) are substantially nega-  
 321 tive. This decrease in tropical temperatures is consistent with the strong tropical upwelling,  
 322 which, in turn led to large negative tropical lower stratosphere H<sub>2</sub>O and O<sub>3</sub> anomalies  
 323 (Fig. 4 and Fig. S3a, c, e in the supplement). Conversely, the tropical cold point tem-  
 324 perature anomalies are warmer and barely exceeding -0.1 K in 2020, consistent with the  
 325 weak tropical residual vertical velocity anomalies (Fig. 4 and Fig. S3b, d, f in the sup-  
 326 plement) and not long lasting tropical O<sub>3</sub> anomalies i.e. about 3 months (Fig. 3 and Fig. S3b,  
 327 d, f in the supplement). These warmer tropical cold point temperatures corroborate the  
 328 slower tropical upwelling and the weaker tropical lower stratospheric H<sub>2</sub>O and O<sub>3</sub> anoma-  
 329 lies in 2020. Interestingly, the differences in the tropical cold point temperature anoma-  
 330 lies between 2016 and 2020 are more pronounced as shown in Figure S3c, d in the sup-  
 331 plement than the differences in the QBO disruption-induced tropical cold point temper-  
 332 ature anomalies (Figure S3e, f in the supplement). This anomalously warmer stratosphere,  
 333 including warmer cold point temperature, in 2020 is consistent with recent findings about  
 334 the impact of Australian wildfire smoke (Khaykin et al., 2020; Yu et al., 2021). Indeed  
 335 using our regression analyses, we can show that the Australian wildfire largely moist-  
 336 ened the lower stratosphere in 2020 by inducing anomalously warmer stratosphere, there-  
 337 fore, hiding the impact of 2019–2020 QBO disruption on H<sub>2</sub>O anomalies (Fig. 3e). The  
 338 removal of Australian wildfire impact allows a better highlight of the weak and similar  
 339 effect of the 2019–2020 QBO disruption on lower stratospheric H<sub>2</sub>O anomalies compared  
 340 to 2015–2016 QBO disruption-induced effect. These differences are also reflected in the  
 341 stratospheric circulation forcing, and we finally investigate the related wave drag changes  
 342 in the following.

343 To investigate the main causes of the stratospheric circulation differences between  
 344 the 2015–2016 and 2019–2020 QBO disruptions, we calculate the planetary and grav-  
 345 ity wave drag. We analyse the differences in terms of wave activities potentially induced  
 346 by specific sea surface conditions such as the unusually warm 2015–2016 El Niño and the  
 347 2019 strong positive Indian Dipole Ocean, which impact tropical convective activities (Jia  
 348 et al., 2014). In addition, we also pay attention to volcanic eruptions and Australian wild-  
 349 fire smoke in 2020, which can impact lower stratospheric temperatures, and therefore,  
 350 lower stratospheric H<sub>2</sub>O and O<sub>3</sub> anomalies. For additional details about the wave de-  
 351 composition please see Diallo et al. (2021) and Ern et al. (2014).

352 The stratospheric circulation as well as its interannual variability are driven by the  
 353 planetary and gravity wave breaking in different stratospheric regions (Haynes et al., 1991;  
 354 Rosenlof & Holton, 1993; Newman & Nash, 2000; Plumb, 2002; Shepherd, 2007). There-  
 355 fore, any changes in wave drag will lead to circulation and composition changes. Figure 5a-  
 356 c show time series of deseasonalized monthly mean tropical net wave forcing (PWD +  
 357 GWD -  $du/dt$ ), planetary wave drag (PWD) and gravity wave drag from the ERA5 re-  
 358 analysis for the 2013–2020 period as a function of time and altitude. Note that the net  
 359 wave forcing is equal to the contribution of Coriolis force plus meridional advection plus  
 360 vertical advection to the momentum balance (Ern et al., 2021). Clearly, the net forcing  
 361 anomalies as well as the planetary and gravity wave drag anomalies exhibit differences  
 362 in strength and depth in the lower stratosphere between the 2015–2016 and 2019–2020

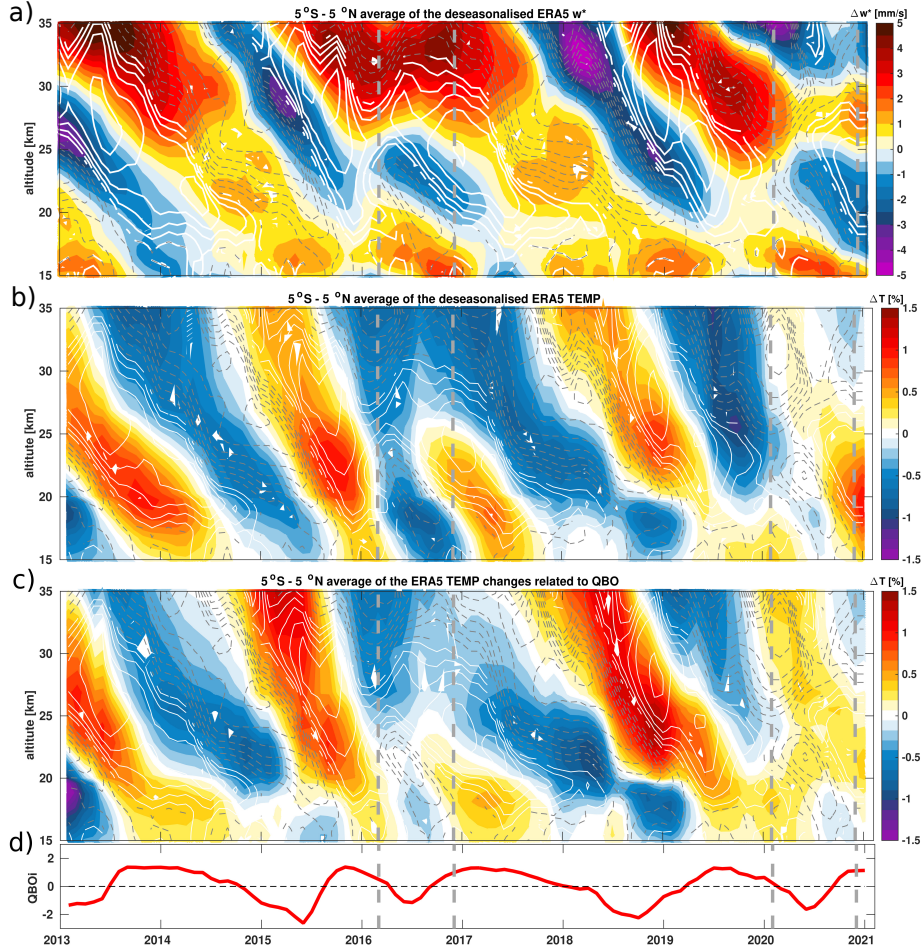


**Figure 4.** Deseasonalized tropical mean residual vertical velocity ( $\overline{w^*}$ ) (a) and temperature anomalies (b) time series from ERA5 for the 2013–2020 period together with the impact of QBO disruptions on the tropical mean temperature anomalies (c) derived from the multiple regression fit as a function of latitude and altitude. (a) Deseasonalized monthly mean tropical upwelling. (b) Deseasonalized monthly mean tropical temperature. (c) QBO disruption impact on monthly mean tropical temperature anomalies. Vertical grey dashed lines indicate the QBO disruption onset and offset years. The lowermost panel shows the QBO index at 50 hPa in red. Monthly averaged zonal mean zonal wind component,  $u$  ( $\text{m s}^{-1}$ ), from ERA5, is overlaid as solid white (westerly) and dashed gray (easterly) lines.

363 QBO disruptions (Fig 5a–c). These differences in wave forcings are even clearer in the  
 364 January-to-June averaged zonal mean net forcing, planetary and gravity wave drag, i.e.  
 365 during six months (January–to–June) of the evolving QBO disruptions (Fig. S4 a–f in  
 366 the supplement). During the 2015–2016 QBO disruption, the net wave forcing is stronger  
 367 and broader in the lower stratosphere than during the 2019–2020 QBO disruption. Par-  
 368 ticularly, the wave breaking near the equatorward flanks of the subtropical jet known  
 369 as BDC forcings region is narrower in 2020 than 2016 (Fig. S4 a, b in the supplement).  
 370 These differences in net forcing are the main cause of a weaker stratospheric circulation  
 371 impact in 2020 than in 2016, therefore, explaining the observed differences in lower strato-  
 372 spheric  $\text{H}_2\text{O}$  and  $\text{O}_3$  anomalies.

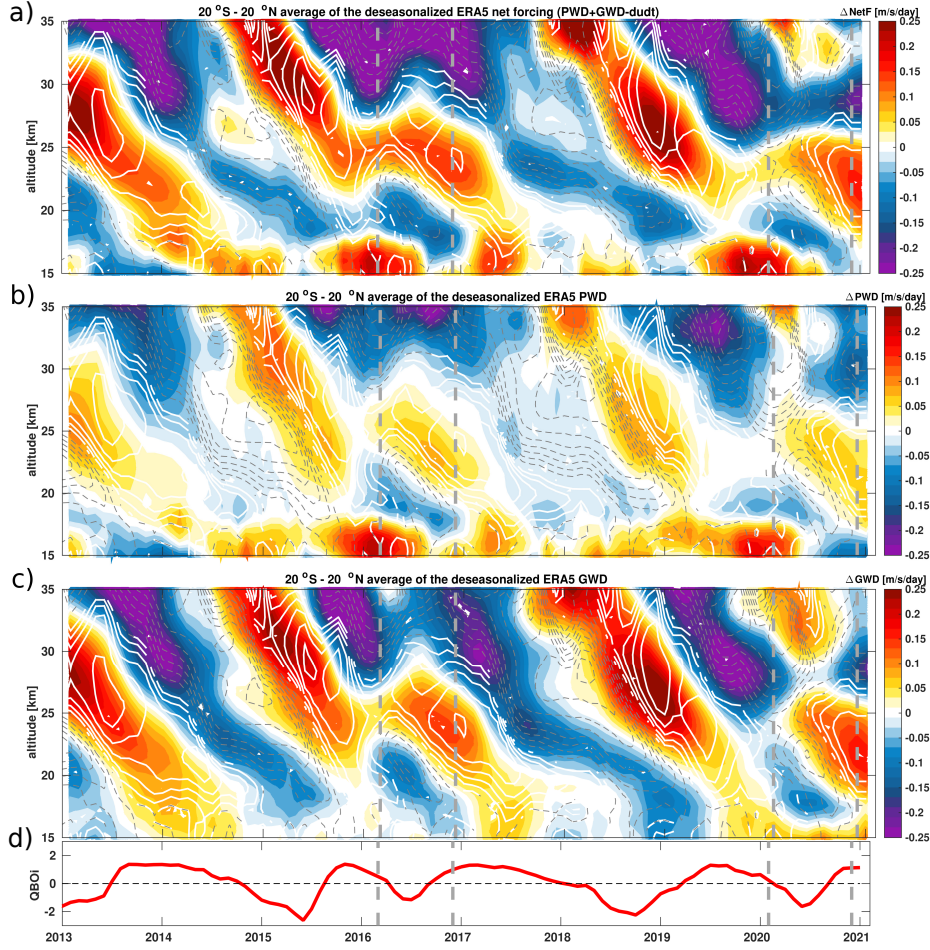


**Figure 5.** Deseasonalized monthly mean tropical net wave forcings (NetF) (a), planetary wave (PWD) (b) drag and gravity wave (GWD) (c) drag time series from ERA5 for the 2013–2020 period as a function of time and altitude. (a) Deseasonalized monthly mean tropical net wave forcing. (b) Deseasonalized monthly mean tropical PWD drag. (c) Deseasonalized monthly mean tropical PWD drag. Vertical grey dashed lines indicate the QBO disruption onset and offset years. The lowermost panel shows the QBO index at 50 hPa in red. Monthly averaged zonal mean zonal wind component,  $u$  ( $\text{m s}^{-1}$ ), from ERA5, is overlaid as solid white (westerly) and dashed gray (easterly) lines.

373 In addition, we show the contribution of planetary (Fig 5b, and Fig. S4c, d) and  
 374 gravity (Fig 5c and Fig. S4e, f) wave drag to better understand the role of each forcing  
 375 during both QBO disruptions. Beside the good agreement in the pattern of planetary  
 376 and gravity wave breaking, our analyses also show differences between the 2015–2016 and  
 377 2019–2020 disruptions in wave drag. The planetary and gravity wave drag indicates stronger  
 378 anomalies in wave dissipation in the lower stratosphere during the 2015–2016 QBO disruption  
 379 than during the 2019–2020 QBO disruption (Fig. 5b, c and Fig. S4c–f in the sup-  
 380 plement). The anomalies in planetary wave dissipation associated with the 2015–2016  
 381 QBO disruption are stronger and extends from the tropics toward the subtropical jet,  
 382 while for the 2019–2020 disruption, these anomalies are weaker and confined to the trop-  
 383 ics. These differences in the strength and depth of the anomalies are even larger in the  
 384 gravity wave drag. During the 2015–2016 QBO disruption, gravity waves break in the

entire lower stratosphere with a maximum occurring near the upper flank of the subtropical jet, a key region for strengthening the shallow branch of the stratospheric circulation (Shepherd & McLandress, 2011; Diallo et al., 2019, 2021) (Fig. 5b and Fig. S4 c, d in the supplement). The differences in the strength and depth of planetary and gravity wave breaking are clearly the main cause of observed differences in the tropical upwelling and cold point temperature between the 2015–2016 and 2019–2020 QBO disruptions. The main cause is a combination of planetary wave dissipation in the tropics and particularly strong gravity wave breaking near the equatorward flanks of the subtropical jet during the 2015–2016 QBO disruption, consistent with previous studies (Kang et al., 2020; Kang & Chun, 2021; Osprey et al., 2016). Note that during the 2015–2016 and 2019–2020 QBO disruptions, the surface conditions were different in terms of natural variability-induced convective activity.

To trace back the potential source of convectively generated wave activities to regional differences, we finally analysed the monthly mean Outgoing Longwave Radiation (OLR) (Fig. S5 a, b in the supplement). Clearly, there are regional differences in the occurrence of strong convective events between the 2015–2016 and 2019–2020 QBO disruptions. During the 2015–2016 QBO disruption, the tropical mean OLR anomalies reveal two active convective regions, namely the East Indian Ocean associated with the negative IOD in 2016, and the Central Pacific Ocean associated with the 2015–2016 El Niño. However, during the 2019–2020 QBO disruption, the tropical mean OLR anomalies show only one strong active convective region that is the West Indian Ocean and East Africa associated with the strong 2019 IOD. Both QBO disruption effects related to OLR variations exhibit strong convective activity in the Indian Ocean, therefore suggesting the importance role of this region may play. This additional information is valuable for better understanding and relating the origin of the QBO disruption and its strength based on regional forcings. This regional forcing and interplay of different modes of climate variability will be presented in further studies.

## 5 Summary and conclusions

Based on an established multiple regression method applied to Aura MLS observations, we found that both the 2015–2016 and 2019–2020 QBO disruptions induced similar structural changes in the lower stratospheric  $\text{H}_2\text{O}$  and  $\text{O}_3$ . Both QBO disruptions induced negative anomalies in  $\text{H}_2\text{O}$  and  $\text{O}_3$ , few months after the sudden shift from the QBO westerly to QBO easterly winds reaches the tropical tropopause. During the boreal winter of 2015–2016 (September 2015–March 2016), the alignment of the strong El Niño with the QBO westerly strongly moistened the lower stratosphere (positive anomalies of more than 20%). Analogously, the alignment of the weak El Niño with the strong QBO westerly and the impact of Australian wildfire smoke strongly moistened the lower stratosphere (positive anomalies of more than 20%) during the boreal winter of 2019–2020 (September 2019–Jun 2020). The sudden shift from the QBO westerly to QBO easterly wind shear reversed the lower stratospheric moistening between the tropopause and 20 km, therefore leading to negative  $\text{H}_2\text{O}$  and  $\text{O}_3$  anomalies by the end of summers 2016 and 2020. These decreases in  $\text{H}_2\text{O}$  and  $\text{O}_3$  mixing ratios are due to a strengthening of the tropical upwelling and cooling tropical cold point temperatures, consistent with the residual vertical velocity and temperature anomalies.

However, major differences occur in the strength and depth of the QBO disruption-induced negative  $\text{H}_2\text{O}$  and  $\text{O}_3$  anomalies between 2016 and 2020. We found that the impact of the 2019–2020 QBO disruption on lower stratospheric  $\text{H}_2\text{O}$  and  $\text{O}_3$  anomalies is weaker and shallower than the 2015–2016 QBO disruption impact. These differences in the strength and depth between the 2015–2016 QBO and 2019–2020 QBO disruption impacts are due to discrepancies in the tropical upwelling and tropical cold point temperature anomalies induced by the differences in wave forcing. The analyses of wave forcings show that net wave forcing in the lower stratosphere, particularly the planetary and

437 gravity wave drag, were stronger during the 2016–2016 QBO disruption than during the  
438 2019–2020 QBO disruption. The differences in planetary wave breaking in the tropical  
439 lower stratosphere and the gravity wave breaking in the equatorward upper flank of the  
440 subtropical jet are the main reasons of the stratospheric circulation and cold point tem-  
441 perature differences between the 2015–2016 and 2019–2020 QBO disruptions and their  
442 impact on lower stratospheric H<sub>2</sub>O and O<sub>3</sub> anomalies.

443 Finally, our results suggest that the interplay of QBO phases with a combination  
444 of ENSO and IOD events, and in particular also wild fires and volcanic eruptions, will  
445 be crucial for the control of the lower stratospheric H<sub>2</sub>O and O<sub>3</sub> budget in a changing  
446 future climate. Especially, when increasing future warming will lead to trends in ENSO  
447 (Timmermann et al., 1999; Cai et al., 2014) and IOD (Ihara et al., 2008) as projected  
448 by climate models, and a related potential increase in wildfire frequency combined with  
449 a decreasing lower stratospheric QBO amplitude (Kawatani & Hamilton, 2013) are ex-  
450 pected in future climate projections. The interplay will change with strong El Niño/negative  
451 IOD and La Niña/strong positive IOD likely controlling the lower stratospheric trace gas  
452 distributions and variability more strongly in a future changing climate. Clearly, both  
453 ENSO and IOD impact on the tropopause height and tropical cold point temperature.  
454 Further analysis is needed using climate model sensitivity simulations to pinpoint the  
455 impact of these future changes in lower stratospheric trace gases and the related radi-  
456 tive feedback.

## 457 Acknowledgments

458 Mohamadou Diallo research position is funded by the Deutsche Forschungsgemeinschaft  
459 (DFG) individual research grant number DI2618/1-1 and Institute of Energy and Cli-  
460 mate Research, Stratosphere (IEK-7), Forschungszentrum in Jülich during which this  
461 work had been carried out. FP is funded by the Helmholtz Association under grant num-  
462 ber VH-NG-1128 (Helmholtz Young Investigators Group A-SPECi). Manfred Ern was  
463 supported by the German Federal Ministry of Education and Research (Bundesminis-  
464 terium für Bildung und Forschung, BMBF) project QUBICC, grant number 01LG1905C,  
465 as part of the Role of the Middle Atmosphere in Climate II (ROMIC-II) programme of  
466 BMBF. We gratefully acknowledge the Earth System Modelling Project (ESM) for fund-  
467 ing this work by providing computing time on the ESM partition of the supercomputer  
468 JUWELS at the Jülich Supercomputing Centre (JSC). Moreover, we particularly thank  
469 the European Centre for Medium-Range Weather Forecasts for providing the ERA5 and  
470 ERA-Interim reanalysis data.

## 471 Data Availability Statement

472 MLS water vapor and ozone data were obtained from the Goddard Earth Sciences  
473 Data and Information Services Center at es Center at doi.10.5067/Aura/MLS/DATA2508  
474 and doi.10.5067/Aura/MLS/DATA2516, respectively. The aerosol optical depth data is  
475 available through Khaykin et al. 2020. The ERA5 reanalysis are available at  
476 <https://apps.ecmwf.int/data-catalogues/era5/?class=ea>, last access: 2nd Febru-  
477 ary 2022, through Hersbach et al., 2020.

## 478 References

- 479 Abalos, M., Ploeger, F., Konopka, P., Randel, W. J., & Serrano, E. (2013). Ozone  
480 seasonality above the tropical tropopause: reconciling the eulerian and lagrangian  
481 perspectives of transport processes. *Atmospheric Chemistry and Physics*, 13(21),  
482 10787–10794. doi: 10.5194/acp-13-10787-2013
- 483 Andrews, D. G., Holton, J. R., & Leovy, C. B. (1987). *Middle atmosphere dynamics*  
484 (Vol. 40). San Diego, USA: Academic Press.

- 485 Anstey, J. A., Banyard, T. P., Butchart, N., Coy, L., Newman, P. A., Osprey, S., &  
486 Wright, C. J. (2021a). Prospect of increased disruption to the qbo in a changing  
487 climate. *Geophys. Res. Lett.*. Retrieved from [https://www.essoar.org/pdf/jrs/](https://www.essoar.org/pdf/jrs/10.1002/essoar.10503358.3)  
488 [10.1002/essoar.10503358.3](https://doi.org/10.1002/essoar.10503358.3) doi: 10.21203/rs.3.rs-86860/v1
- 489 Anstey, J. A., Banyard, T. P., Butchart, N., Coy, L., Newman, P. A., Osprey, S., &  
490 Wright, C. J. (2021b). Quasi-biennial oscillation disrupted by abnormal southern  
491 hemisphere stratosphere. *Geophys. Res. Lett.*. Retrieved from [https://doi.org/](https://doi.org/10.1002/essoar.10503358.2)  
492 [10.1002/essoar.10503358.2](https://doi.org/10.1002/essoar.10503358.2) doi: 10.1002/essoar.10503358.2
- 493 Baldwin, M. P., Gray, L. J., Dunkerton, T. J., Hamilton, K., Haynes, P. H., Ran-  
494 del, W. J., ... Takahashi, M. (2001). The quasi-biennial oscillation. *Reviews of*  
495 *Geophysics*, *39*(2), 179–229. doi: 10.1029/1999RG000073
- 496 Barton, C. A., & McCormack, J. P. (2017). Origin of the 2016 QBO Disruption and  
497 Its Relationship to Extreme El Niño Events. *Geophys. Res. Lett.*. doi: 10.1002/  
498 2017GL075576
- 499 Butchart, N., & Scaife, A. A. (2001). Removal of chlorofluorocarbons by increased  
500 mass exchange between the stratosphere and troposphere in a changing climate. ,  
501 *J*, *4*(10), 799–802. doi: 10.1038/35071047
- 502 Cai, W., Borlace, S., Lengaigne, M., van Rensch, P., Collins, M., Vecchi, G., ... Jin,  
503 F.-F. (2014). Increasing frequency of extreme El Niño events due to greenhouse  
504 warming. *Nat. Clim. Change*, *4*(2), 111–116. doi: 10.1038/nclimate2100
- 505 Christiansen, B., Yang, S., & Madsen, M. S. (2016). Do strong warm ENSO events  
506 control the phase of the stratospheric QBO? *Geophys. Res. Lett.*, *43*(19), 10,489–  
507 10,495. doi: 10.1002/2016GL070751
- 508 Coy, L., Newman, P. A., Pawson, S., & Lait, L. R. (2017). Dynamics of the Dis-  
509 rupted 2015/16 Quasi-Biennial Oscillation. *J. Clim.*, *30*(15), 5661–5674. doi: 10  
510 .1175/JCLI-D-16-0663.1
- 511 DallaSanta, K., Orbe, C., Rind, D., Nazarenko, L., & Jonas, J. (2021). Response  
512 of the quasi-biennial oscillation to historical volcanic eruptions. *Geophysical*  
513 *Research Letters*, *48*(20), e2021GL095412. Retrieved from [https://agupubs](https://agupubs.onlinelibrary.wiley.com/doi/abs/10.1029/2021GL095412)  
514 [.onlinelibrary.wiley.com/doi/abs/10.1029/2021GL095412](https://agupubs.onlinelibrary.wiley.com/doi/abs/10.1029/2021GL095412) (e2021GL095412  
515 2021GL095412) doi: <https://doi.org/10.1029/2021GL095412>
- 516 Damadeo, R. P., Zawodny, J. M., & Thomason, L. W. (2014). Reevaluation  
517 of stratospheric ozone trends from SAGE II data using a simultaneous tem-  
518 poral and spatial analysis. *Atmos. Chem. Phys.*, *14*(24), 13455–13470. doi:  
519 10.5194/acp-14-13455-2014
- 520 Dessler, A. E., Schoeberl, M. R., Wang, T., Davis, S. M., & Rosenlof, K. H. (2013).  
521 Stratospheric water vapor feedback. *Proceed. Nat. Acad. Sci.*, *110* 45, 18087–91.
- 522 Diallo, M., Ern, M., & Ploeger, F. (2021). The advective brewer–dobson circulation  
523 in the era5 reanalysis: climatology, variability, and trends. *Atmospheric Chemistry*  
524 *and Physics*, *21*(10), 7515–7544. Retrieved from [https://acp.copernicus.org/](https://acp.copernicus.org/articles/21/7515/2021/)  
525 [articles/21/7515/2021/](https://acp.copernicus.org/articles/21/7515/2021/) doi: 10.5194/acp-21-7515-2021
- 526 Diallo, M., Konopka, P., Santee, M. L., Müller, R., Tao, M., Walker, K. A., ...  
527 Ploeger, F. (2019). Structural changes in the shallow and transition branch of  
528 the brewer–dobson circulation induced by el niño. *Atmospheric Chemistry and*  
529 *Physics*, *19*(1), 425–446. Retrieved from [https://www.atmos-chem-phys.net/](https://www.atmos-chem-phys.net/19/425/2019/)  
530 [19/425/2019/](https://www.atmos-chem-phys.net/19/425/2019/) doi: 10.5194/acp-19-425-2019
- 531 Diallo, M., Ploeger, F., Konopka, P., Birner, T., Müller, R., Riese, M., ... Jegou,  
532 F. (2017). Significant contributions of volcanic aerosols to decadal changes in the  
533 stratospheric circulation. *Geophysical Research Letters*, *44*(20), 10,780–10,791.  
534 Retrieved from [https://agupubs.onlinelibrary.wiley.com/doi/abs/10.1002/](https://agupubs.onlinelibrary.wiley.com/doi/abs/10.1002/2017GL074662)  
535 [2017GL074662](https://agupubs.onlinelibrary.wiley.com/doi/abs/10.1002/2017GL074662) doi: 10.1002/2017GL074662
- 536 Diallo, M., Riese, M., Birner, T., Konopka, P., Müller, R., Hegglin, M. I., ...  
537 Ploeger, F. (2018). Response of stratospheric water vapor and ozone to  
538 the unusual timing of el niño and the qbo disruption in 2015–2016. *Atmo-*

- 539        *spheric Chemistry and Physics*, 18(17), 13055–13073. Retrieved from [https://](https://www.atmos-chem-phys.net/18/13055/2018/)  
 540        [www.atmos-chem-phys.net/18/13055/2018/](https://www.atmos-chem-phys.net/18/13055/2018/) doi: 10.5194/acp-18-13055-2018
- 541 Dunkerton, T. J. (1980). A Lagrangian mean theory of wave, mean-Flow interaction  
 542        with applications to nonacceleration and its breakdown. *Rev. of Geophys.*, 18(2),  
 543        387–400. doi: 10.1029/RG018i002p00387
- 544 Dunkerton, T. J. (2016). The quasi-biennial oscillation of 2015–2016: Hic-  
 545        cup or death spiral? *Geophys. Res. Lett.*, 43(19), 10,547–10,552. doi:  
 546        10.1002/2016GL070921
- 547 Ern, M., Diallo, M., Preusse, P., Mlynczak, M. G., Schwartz, M. J., Wu, Q.,  
 548        & Riese, M. (2021). The semiannual oscillation (sao) in the tropical mid-  
 549        dle atmosphere and its gravity wave driving in reanalyses and satellite ob-  
 550        servations. *Atmos. Chem. Phys.*, 21(18), 13763–13795. Retrieved from  
 551        <https://acp.copernicus.org/articles/21/13763/2021/> doi: 10.5194/  
 552        acp-21-13763-2021
- 553 Ern, M., Ploeger, F., Preusse, P., Gille, J. C., Gray, L. J., Kalisch, S., ... Riese, M.  
 554        (2014). Interaction of gravity waves with the QBO: A satellite perspective. *J.*  
 555        *Geophys. Res.: Atmospheres*, 119(5), 2329–2355. doi: 10.1002/2013JD020731
- 556 Forster, P. M., & Shine, K. P. (1999). Stratospheric water vapour changes as a pos-  
 557        sible contributor to observed stratospheric cooling. *Geophys. Res. Lett.*, 26(21),  
 558        3309–3312. doi: 10.1029/1999GL010487
- 559 Forster, P. M., & Shine, K. P. (2002). Assessing the climate impact of trends  
 560        in stratospheric water vapor. *Geophys. Res. Lett.*, 29(6). doi: 10.1029/  
 561        2001GL013909
- 562 Friston, K., Ashburner, J., Kiebel, S. J., Nichols, T. E., & Penny, W. D. (Eds.).  
 563        (2007). *Statistical parametric mapping: The analysis of functional brain*  
 564        *images*. Academic Press. Retrieved from [http://store.elsevier.com/](http://store.elsevier.com/product.jsp?isbn=9780123725608)  
 565        [product.jsp?isbn=9780123725608](http://store.elsevier.com/product.jsp?isbn=9780123725608)
- 566 Fueglistaler, S., Dessler, A. E., Dunkerton, T. J., Folkins, I., Fu, Q., & Mote, P. W.  
 567        (2009, February). Tropical tropopause layer. *Rev. Geophys.*, 47, G1004+. doi:  
 568        10.1029/2008RG000267
- 569 Garfinkel, C. I., Hurwitz, M. M., Oman, L. D., & Waugh, D. W. (2013). Contrast-  
 570        ing Effects of Central Pacific and Eastern Pacific El Niño on stratospheric water  
 571        vapor. *Geophys. Res. Lett.*, 40(15), 4115–4120. doi: 10.1002/grl.50677
- 572 Geller, M. A., Zhou, X., & Zhang, M. (2002). Simulations of the Interannual Vari-  
 573        ability of Stratospheric Water Vapor. *J. Atmos. Sci.*, 59(6), 1076–1085. doi: 10  
 574        .1175/1520-0469(2002)059<\$(\$1076:SOTIVO)\$>\$2.0.CO;2
- 575 Gettelman, A., Hoor, P., Pan, L. L., Randel, W. J., Hegglin, M. I., & Birner, T.  
 576        (2011). The extratropical upper troposphere and lower stratosphere. *Rev. Geo-*  
 577        *phys.*, 49, RG3003. doi: 10.1029/2011RG000355
- 578 Grimshaw, R. (1984). Wave Action and Wave-Mean Flow Interaction, with Applica-  
 579        tion to Stratified Shear Flows. *Annual Rev. of Fluid Mech.*, 16(1), 11–44. doi: 10  
 580        .1146/annurev.fl.16.010184.000303
- 581 Hartmann, D. L., Holton, J. R., & Fu, Q. (2001). The heat balance of the tropi-  
 582        cal tropopause, cirrus, and stratospheric dehydration. *Geophys. Res. Lett.*, 28(10),  
 583        1969–1972. doi: 10.1029/2000GL012833
- 584 Haynes, P. H., McIntyre, M. E., Shepherd, T. G., Marks, C. J., & Shine, K. P.  
 585        (1991). On the “downward control” of extratropical diabatic circulations  
 586        by eddy-induced mean zonal forces. *J. Atmos. Sci.*, 48(4), 651–678. doi:  
 587        10.1175/1520-0469(1991)048<\$(\$0651:OTCOED)\$>\$2.0.CO;2
- 588 Haynes, P. H., & Shuckburgh, E. (2000). Effective diffusivity as a diagnostic of  
 589        atmospheric transport 2. Troposphere and lower stratosphere. *J. Geophys. Res.*,  
 590        105(D18), 22795–22810. doi: 10.1029/2000JD900092
- 591 Hegglin, M. I., Tegtmeier, S., Anderson, J., Bourassa, A. E., Brohede, S., De-  
 592        genstein, D., ... Weigel, K. (2021). Overview and update of the sparc data

- 593 initiative: comparison of stratospheric composition measurements from satel-  
 594 lite limb sounders. *Earth Syst. Sci. Data*, 13(5), 1855–1903. Retrieved from  
 595 <https://essd.copernicus.org/articles/13/1855/2021/> doi: 10.5194/  
 596 essd-13-1855-2021
- 597 Hegglin, M. I., Tegtmeier, S., Anderson, J., Froidevaux, L., Fuller, R., Funke, B., ...  
 598 Weigel, K. (2013). Sparc data initiative: Comparison of water vapor climatolo-  
 599 gies from international satellite limb sounders. *J. Geophys. Res.: Atmospheres*,  
 600 118(20), 11,824–11,846. doi: 10.1002/jgrd.50752
- 601 Hersbach, H., Bell, B., Berrisford, P., Hirahara, S., Horányi, A., Muñoz-Sabater, J.,  
 602 ... Thépaut, J.-N. (2020). The era5 global reanalysis. *Q. J. R. Meteorol. Soc.*,  
 603 n/a(n/a). Retrieved from [https://rmets.onlinelibrary.wiley.com/doi/abs/](https://rmets.onlinelibrary.wiley.com/doi/abs/10.1002/qj.3803)  
 604 10.1002/qj.3803 doi: 10.1002/qj.3803
- 605 Hitchcock, P., Haynes, P. H., Randel, W. J., & Birner, T. (2018). The Emergence of  
 606 Shallow Easterly Jets within QBO Westerlies. *J. Atmos. Sci.*, 75(1), 21–40. doi:  
 607 10.1175/JAS-D-17-0108.1
- 608 Holton, J. R. (1979). Equatorial Wave-Mean Flow Interaction: A Numerical Study  
 609 of the Role of Latitudinal Shear. *J. Atmos. Sci.*, 36(6), 1030–1040. doi: 10.1175/  
 610 1520-0469(1979)036<\$1030:EWMFIA>\$2.0.CO;2
- 611 Holton, J. R., & Gettelman, A. (2001). Horizontal transport and the dehy-  
 612 dration of the stratosphere. *Geophys. Res. Lett.*, 28(14), 2799–2802. doi:  
 613 10.1029/2001GL013148
- 614 Hu, D., Tian, W., Guan, Z., Guo, Y., & Dhomse, S. (2016). Longitudinal Asym-  
 615 metric Trends of Tropical Cold-Point Tropopause Temperature and Their  
 616 Link to Strengthened Walker Circulation. *J. Clim.*, 29(21), 7755–7771. doi:  
 617 10.1175/JCLI-D-15-0851.1
- 618 Ihara, C., Kushnir, Y., & Cane, M. A. (2008). Warming trend of the indian ocean  
 619 sst and indian ocean dipole from 1880 to 2004. *J. of Clim.*, 21(10), 2035 - 2046.  
 620 Retrieved from [https://journals.ametsoc.org/view/journals/clim/21/10/](https://journals.ametsoc.org/view/journals/clim/21/10/2007jcli1945.1.xml)  
 621 2007jcli1945.1.xml doi: 10.1175/2007JCLI1945.1
- 622 Jensen, E. J., Toon, O. B., Pfister, L., & Selkirk, H. B. (1996). Dehydration  
 623 of the upper troposphere and lower stratosphere by subvisible cirrus clouds  
 624 near the tropical tropopause. *Geophys. Res. Lett.*, 23(8), 825–828. doi:  
 625 10.1029/96GL00722
- 626 Jia, J. Y., Preusse, P., Ern, M., Chun, H.-Y., Gille, J. C., Eckermann, S. D., &  
 627 Riese, M. (2014). Sea surface temperature as a proxy for convective grav-  
 628 ity wave excitation: a study based on global gravity wave observations in the  
 629 middle atmosphere. *Annales Geophysicae*, 32(11), 1373–1394. Retrieved  
 630 from <https://angeo.copernicus.org/articles/32/1373/2014/> doi:  
 631 10.5194/angeo-32-1373-2014
- 632 Kalnay, E., Kanamitsu, M., Kistler, R., Collins, W., Deaven, D., Gandin, L., ...  
 633 Joseph, D. (1996). The ncep/ncar 40-year reanalysis project. *Bulletin of the*  
 634 *American Meteorological Society*, 77(3), 437 - 472. Retrieved from [https://](https://journals.ametsoc.org/view/journals/bams/77/3/1520-0477_1996_077_0437_tnyr_2_0_co_2.xml)  
 635 [journals.ametsoc.org/view/journals/bams/77/3/1520-0477\\_1996\\_077\\_0437](https://journals.ametsoc.org/view/journals/bams/77/3/1520-0477_1996_077_0437_tnyr_2_0_co_2.xml)  
 636 [\\_tnyrp\\_2\\_0\\_co\\_2.xml](https://journals.ametsoc.org/view/journals/bams/77/3/1520-0477_1996_077_0437_tnyr_2_0_co_2.xml) doi: 10.1175/1520-0477(1996)077<0437:TNYRP>2.0.CO;2
- 637 Kang, M.-J., & Chun, H.-Y. (2021). Contributions of equatorial planetary waves and  
 638 small-scale convective gravity waves to the 2019/20 qbo disruption. *Atmos. Chem.*  
 639 *Phys.*, 2021, 1–33. Retrieved from [https://acp.copernicus.org/preprints/acp-](https://acp.copernicus.org/preprints/acp-2021-85/)  
 640 [2021-85/](https://acp.copernicus.org/preprints/acp-2021-85/) doi: 10.5194/acp-2021-85
- 641 Kang, M.-J., Chun, H.-Y., & Garcia, R. R. (2020). Role of equatorial waves  
 642 and convective gravity waves in the 2015/16 quasi-biennial oscillation disrup-  
 643 tion. *Atmos. Chem. Phys.*, 20(23), 14669–14693. Retrieved from [https://acp-](https://acp.copernicus.org/articles/20/14669/2020/)  
 644 [copernicus.org/articles/20/14669/2020/](https://acp.copernicus.org/articles/20/14669/2020/) doi: 10.5194/acp-20-14669-2020
- 645 Kawatani, Y., & Hamilton, K. (2013). Weakened stratospheric quasibiennial oscilla-  
 646 tion driven by increased tropical mean upwelling. *Nature*, 497, 478–481. doi: doi:

- 647 10.1038/nature12140
- 648 Kawatani, Y., Hamilton, K., & Watanabe, S. (2011). The Quasi-Biennial Oscil-  
649 lation in a Double CO<sub>2</sub> Climate. *J. Atmos. Sci.*, *68*(2), 265-283. doi: 10.1175/  
650 2010JAS3623.1
- 651 Khaykin, S., Legras, B., & Bucci, S. e. a. (2020). The 2019/20 australian wildfires  
652 generated a persistent smoke-charged vortex rising up to 35km altitude. *Commun.*  
653 *Earth Environ.*, *1*(22). doi: 10.1038/s43247-020-00022-5
- 654 Kim, J., & Alexander, M. J. (2015). Direct impacts of waves on tropical cold point  
655 tropopause temperature. *Geophys. Res. Lett.*, *42*(5), 1584-1592. doi: [https://doi](https://doi.org/10.1002/2014GL062737)  
656 [.org/10.1002/2014GL062737](https://doi.org/10.1002/2014GL062737)
- 657 Kim, J., & Son, S.-W. (2012). Tropical Cold-Point Tropopause: Climatology,  
658 Seasonal Cycle, and Intraseasonal Variability Derived from COSMIC GPS Ra-  
659 dio Occultation Measurements. *Journal of Climate*, *25*(15), 5343-5360. doi:  
660 10.1175/JCLI-D-11-00554.1
- 661 Kroll, C. A., Dacie, S., Azoulay, A., Schmidt, H., & Timmreck, C. (2020). The  
662 impact of volcanic eruptions of different magnitude on stratospheric water vapour  
663 in the tropics. *Atmos. Chem. Phys.*, *2020*, 1-45. Retrieved from [https://](https://acp.copernicus.org/preprints/acp-2020-1191/)  
664 [acp.copernicus.org/preprints/acp-2020-1191/](https://acp.copernicus.org/preprints/acp-2020-1191/) doi: 10.5194/acp-2020-1191
- 665 Liess, S., & Geller, M. A. (2012). On the relationship between QBO and distribu-  
666 tion of tropical deep convection. *J. Geophys. Res.: Atmospheres*, *117*(D3). doi: 10  
667 .1029/2011JD016317
- 668 Livesey, N. J., Read, W. G., Wagner, P. A., Froidevaux, L., Lambert, A., Manney,  
669 G. L., ... Martinez, E. (2017). Aura Microwave Limb Sounder (MLS) Version  
670 4.2x Level 2 data quality and description document. *Tech. Rep. JPL D-33509*  
671 *Rev. C*, 1-169. doi: 10.5194/acp-15-9945-2015
- 672 Newman, P. A., Coy, L., Pawson, S., & Lait, L. R. (2016). The anomalous change  
673 in the QBO in 2015-2016. *Geophys. Res. Lett.*, *43*(16), 8791-8797. doi: 10.1002/  
674 2016GL070373
- 675 Newman, P. A., & Nash, E. R. (2000). Quantifying the wave driving of the strato-  
676 sphere. *J. Geophys. Res.: Atmospheres*, *105*(D10), 12485-12497. doi: 10.1029/  
677 1999JD901191
- 678 Niwano, M., Yamazaki, K., & Shiotani, M. (2003, December). Seasonal and  
679 qbo variations of ascent rate in the tropical lower stratosphere as inferred from  
680 uars haloe trace gas data. *J. Geophys. Res.*, *108*(D24), 4794. (4794) doi:  
681 10.1029/2003JD003871
- 682 Nowack, P., Abraham, N., Maycock, A., Braesicke, P., Gregory, J., Joshi, M., ...  
683 Pyle, J. (2015, January). A large ozone-circulation feedback and its implica-  
684 tions for global warming assessments. *Nature Climate Change*, *5*, 41-45. doi:  
685 10.1038/NCLIMATE2451
- 686 Osprey, S. M., Butchart, N., Knight, J. R., Scaife, A. A., Hamilton, K., Anstey,  
687 J. A., ... Zhang, C. (2016, September 08). An unexpected disruption of the  
688 atmospheric quasi-biennial oscillation. *Science*. doi: 10.1126/science.aah4156
- 689 Plumb, R. A. (2002). Stratospheric transport. *J. Meteor. Soc. Japan*, *80*, 793-809.
- 690 Randel, W. J., Park, M., Wu, F., & Livesey, N. (2007). A Large Annual Cycle in  
691 Ozone above the Tropical Tropopause Linked to the Brewer Dobson Circulation.  
692 *J. Atmos. Sci.*, *64*(12), 4479-4488. doi: 10.1175/2007JAS2409.1
- 693 Randel, W. J., & Thompson, A. M. (2011). Interannual variability and trends  
694 in tropical ozone derived from sage ii satellite data and shadoz ozonesondes.  
695 *Journal of Geophysical Research: Atmospheres*, *116*(D7). Retrieved from  
696 <https://agupubs.onlinelibrary.wiley.com/doi/abs/10.1029/2010JD015195>  
697 doi: <https://doi.org/10.1029/2010JD015195>
- 698 Riese, M., Ploeger, F., Rap, A., Vogel, B., Konopka, P., Dameris, M., & Forster,  
699 P. (2012). Impact of uncertainties in atmospheric mixing on simulated  
700 utls composition and related radiative effects. *J. Geophys. Res.*, *117*. doi:

- 10.1029/2012JD017751
- Rosenlof, K., & Holton, J. (1993). Estimates of the stratospheric residual circulation using the downward control principle. *J. Geophys. Res.*, *98*, 10,465–10,479.
- Saji, N., Goswami, B., Vinayachandran, P., & Yamagata, T. (1999, September). A dipole mode in the tropical Indian Ocean. *Nature*, *401*(6751), 360–363. Retrieved from <https://doi.org/10.1038/43854> doi: 10.1038/43854
- Santee, M. L., Manney, G. L., Livesey, N. J., Schwartz, M. J., Neu, J. L., & Read, W. G. (2017). A comprehensive overview of the climatological composition of the Asian summer monsoon anticyclone based on 10 years of Aura Microwave Limb Sounder measurements. *J. Geophys. Res.: Atmospheres*, *122*(10), 5491–5514. doi: 10.1002/2016JD026408
- Saravanan, R. (1990). A Multiwave Model of the Quasi-biennial Oscillation. *J. Atmos. Sci.*, *47*(21), 2465–2474. doi: 10.1175/1520-0469(1990)047<2465:AMMOTQ>2.0.CO;2
- Schirber, S. (2015). Influence of ENSO on the QBO: Results from an ensemble of idealized simulations. *J. Geophys. Res.: Atmospheres*, *120*(3), 1109–1122. doi: 10.1002/2014JD022460
- Schoeberl, M. R., & Dessler, A. E. (2011, August). Dehydration of the stratosphere. *Atmos. Chem. Phys.*, *11*, 8433–8446. doi: 10.5194/acp-11-8433-2011
- Shepherd, T. G. (2007). Transport in the middle atmosphere. *J. Meteorol. Soc. of Japan. Ser. II*, *85B*, 165–191. doi: 10.2151/jmsj.85B.165
- Shepherd, T. G., & McLandress, C. (2011). A robust mechanism for strengthening of the Brewer–Dobson circulation in response to climate change: Critical-layer control of subtropical wave breaking. *J. Atmos. Sci.*, *68*(4), 784–797. Retrieved from <https://doi.org/10.1175/2010JAS3608.1> doi: 10.1175/2010JAS3608.1
- Smith, J. W., Haynes, P. H., Maycock, A. C., Butchart, N., & Bushell, A. C. (2021). Sensitivity of stratospheric water vapour to variability in tropical tropopause temperatures and large-scale transport. *Atmospheric Chemistry and Physics*, *21*(4), 2469–2489. Retrieved from <https://acp.copernicus.org/articles/21/2469/2021/> doi: 10.5194/acp-21-2469-2021
- Solomon, S., Rosenlof, K. H., Portmann, R. W., Daniel, S. M., J. S. Davis, Sanford, T., & Plattner, G.-K. (2010). Contributions of Stratospheric Water Vapor to Decadal Changes in the Rate of Global Warming. *Science*, *327*(5970), 1219–1223. doi: 10.1126/science.1182488
- Son, S.-W., Lim, Y., Yoo, C., Hendon, H. H., & Kim, J. (2017). Stratospheric control of the Madden–Julian oscillation. *Journal of Climate*, *30*(6), 1909–1922. Retrieved from <https://journals.ametsoc.org/view/journals/clim/30/6/jcli-d-16-0620.1.xml> doi: 10.1175/JCLI-D-16-0620.1
- Taguchi, M. (2010). Observed connection of the stratospheric quasi-biennial oscillation with El Niño–Southern Oscillation in radiosonde data. *J. Geophys. Res.: Atmospheres*, *115*(D18). doi: 10.1029/2010JD014325
- Tao, M., Konopka, P., Ploeger, F., Yan, X., Wright, J. S., Diallo, M., ... Riese, M. (2019). Multitimescale variations in modeled stratospheric water vapor derived from three modern reanalysis products. *Atmos. Chem. Phys.*, *19*(9), 6509–6534. Retrieved from <https://acp.copernicus.org/articles/19/6509/2019/> doi: 10.5194/acp-19-6509-2019
- Thomason, L. W., Ernest, N., Millán, L., Rieger, L., Bourassa, A., Vernier, J.-P., ... Peter, T. (2018). A global space-based stratospheric aerosol climatology: 1979–2016. *Earth Sys. Sci. Data*, *10*(1), 469–492. doi: 10.5194/essd-10-469-2018
- Tian, E. W., Su, H., Tian, B., & Jiang, J. H. (2019). Interannual variations of water vapor in the tropical upper troposphere and the lower and middle stratosphere and their connections to ENSO and QBO. *Atmospheric Chemistry and Physics*, *19*(15), 9913–9926. Retrieved from <https://acp.copernicus.org/articles/19/9913/2019/> doi: 10.5194/acp-19-9913-2019

- 755 Timmermann, A., Oberhuber, J., Bacher, A., Esch, M., Latif, M., & Roeckner, E.  
756 (1999). El Niño, La Nina, and the Southern Oscillation. *Nature*, *398*(6729),  
757 904-905. doi: 10.1038/19505
- 758 Tweedy, O. V., Kramarova, N. A., Strahan, S. E., Newman, P. A., Coy, L., Randel,  
759 W. J., ... Frith, S. M. (2017). Response of trace gases to the disrupted 2015–  
760 2016 quasi-biennial oscillation. *Atmos. Chem. Phys.*, *17*(11), 6813–6823. doi:  
761 10.5194/acp-17-6813-2017
- 762 von Storch, H., & Zwiers, F. W. (1999). *Statistical analysis in climate research*.  
763 Cambridge Univ. Press.
- 764 WMO. (2018). *Scientific Assessment of Ozone Depletion: 2018* (Global Ozone Re-  
765 search and Monitoring Project - Report No. 58). Geneva: WMO (World Meteorolo-  
766 gical Organization).
- 767 Wolter, K., & Timlin, M. S. (2011). El Nino/Southern Oscillation behaviour since  
768 1871 as diagnosed in an extended multivariate ENSO index (MEI.ext). *Int. J. Cli-*  
769 *matol.*, *31*, 1074–1087. doi: 10.1002/joc.2336
- 770 Yu, P., Davis, S. M., Toon, O. B., Portmann, R. W., Bardeen, C. G., Barnes, J. E.,  
771 ... Rosenlof, K. H. (2021). Persistent stratospheric warming due to 2019-2020  
772 australian wildfire smoke. *Geophys. Res. Lett.*, *48*(7), e2021GL092609. Re-  
773 trieved from [https://agupubs.onlinelibrary.wiley.com/doi/abs/10.1029/](https://agupubs.onlinelibrary.wiley.com/doi/abs/10.1029/2021GL092609)  
774 [2021GL092609](https://agupubs.onlinelibrary.wiley.com/doi/abs/10.1029/2021GL092609) (e2021GL092609 2021GL092609) doi: [https://doi.org/10.1029/](https://doi.org/10.1029/2021GL092609)  
775 [2021GL092609](https://doi.org/10.1029/2021GL092609)